

# Multi-Granular Spatio-Temporal Token Merging for Training-Free Acceleration of Video LLMs

Jeongseok Hyun<sup>1\*</sup> Sukjun Hwang<sup>2</sup> Su Ho Han<sup>1</sup> Taeoh Kim<sup>3</sup> Inwoong Lee<sup>3</sup>  
 Dongyoon Wee<sup>3</sup> Joon-Young Lee<sup>4</sup> Seon Joo Kim<sup>1†</sup> Minho Shim<sup>3†</sup>  
<sup>1</sup>Yonsei University <sup>2</sup>Carnegie Mellon University <sup>3</sup>NAVER Cloud <sup>4</sup>Adobe Research

## Abstract

Video large language models (LLMs) achieve strong video understanding by leveraging a large number of spatio-temporal tokens, but suffer from quadratic computational scaling with token count. To address this, we propose a training-free spatio-temporal token merging method, named STTM. Our key insight is to exploit local spatial and temporal redundancy in video data which has been overlooked in prior work. STTM first transforms each frame into multi-granular spatial tokens using a coarse-to-fine search over a quadtree structure, then performs directed pairwise merging across the temporal dimension. This decomposed merging approach outperforms existing token reduction methods across six video QA benchmarks. Notably, STTM achieves a 2× speed-up with only a 0.5% accuracy drop under a 50% token budget, and a 3× speed-up with just a 2% drop under a 30% budget. Moreover, STTM is query-agnostic, allowing KV cache reuse across different questions for the same video. The project page is available at <https://www.jshyun.me/projects/sttm>.

## 1. Introduction

Integrating visual understanding capabilities into Large Language Models (LLMs) has led to significant advances in multimodal systems [1, 11, 17, 45, 47, 50, 56]. However, Video LLMs, which extend these capabilities to video understanding, face unique computational challenges due to the inherently large number of visual tokens required to represent spatio-temporal information [7, 26, 32, 35, 39, 58].

Early video LLMs [26, 27, 39, 58] reduce token count by training abstractors (e.g., Q-Former [25]) to compress visual information. FlashAttention (FA) [9, 10] reduces attention’s quadratic memory cost to linear, enabling the training of long-context LLMs. Building on this, LLaVA-style [29] video LLMs use linear projectors that preserve

\*This work was done during an internship at NAVER Cloud.

†Co-corresponding authors.

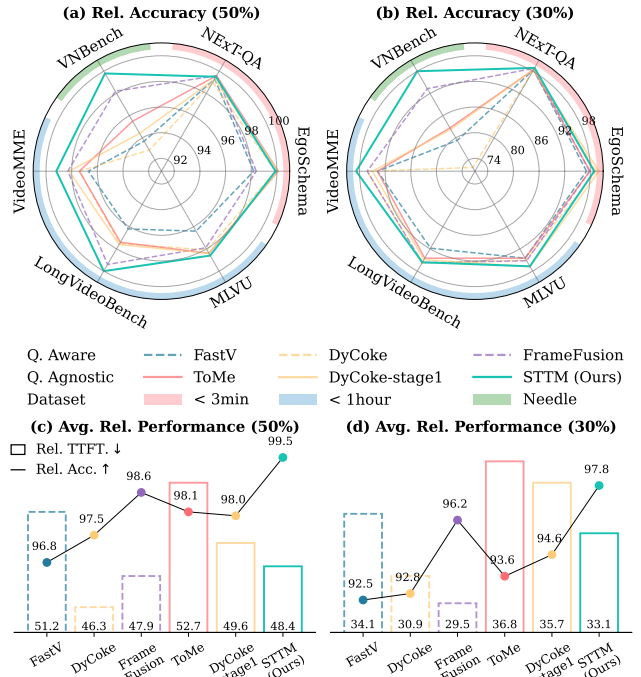


Figure 1. Comparison of training-free token reduction methods using LLaVA-Video-7B under 50% and 30% pre-filling token budgets. Query-aware (Q. Aware) methods require re-computation for each new query, whereas query-agnostic methods support KV-cache reuse. The evaluated video QA datasets cover short (<3 min), long (<1 hr), and needle-in-a-haystack (NIAH) videos. (a, b): Per-dataset accuracy. (c, d): Average results across all.

high-resolution spatial features and deliver strong performance [59, 60]. More recently, Ring Attention [31] extends FA [9] across GPUs, enabling very long-context models, such as LWM [30] and LongVILA [7], to process hour-long videos with high spatial and temporal resolution features.

Long latency remains a key bottleneck for deploying video LLMs. Attention FLOPs still scale quadratically with token count, and long video contexts must be processed in full to pre-fill Key-Value (KV) states before answering any question [34]. In practice (e.g., Gemini [16]), KV states for the video are cached to avoid recomputation for subse-

quent queries, supporting efficient multi-turn querying over a shared video context. However, existing training-free token reduction methods [6, 15, 20, 43], which avoid the overhead of retraining, overlook this scenario and instead focus on query-aware strategies that discard video tokens based on attention scores between the video and the query, without preserving KV cache reusability.

Designing a query-agnostic token reduction method is essential for enabling KV cache reuse, but it is challenging due to the lack of signals to guide token selection. VideoMAE [12, 46] demonstrates that videos can be reconstructed from a lower token ratio than images, highlighting the inherently redundant nature of video content due to its spatio-temporal continuity. However, existing training-free token reduction methods do not explicitly leverage this spatio-temporal structure [6, 15, 38, 43, 49]. To address this, we propose a novel spatio-temporal token merging method, named *STTM*, which is applied at an early layer of the LLM. *STTM* performs decomposed merging: it first merges tokens along the spatial dimension, followed by merging along the temporal dimension.

To perform spatial merging, we build a multi-level quadtree for each video frame, linking each parent node to its four child nodes. A parent node’s token is retained at the coarsest level when its similarity to all four child nodes exceeds a threshold. Regions containing fine-grained details – indicated by low similarity – are subdivided to the next finer level to preserve high-frequency information. Consequently, each frame is represented by multi-granular spatial tokens, capturing both coarse and fine detail.

Extending spatial merging to the spatio-temporal domain is not trivial, due to varying spatial granularities across frames. To handle this challenge, we exploit spatio-temporal locality by restricting merging candidates to spatially overlapping tokens between consecutive frames. Unlike prior temporal-only methods that compare single-granularity tokens across adjacent frames [15], our approach fully leverages the spatial structure and temporal continuity in video data to guide token merging.

After comparing spatially overlapping tokens across time, similar token pairs are chained into spatio-temporal graphs. Within each graph, nodes are merged into a single token representing a token tracklet, with merging directed toward the earlier frame. This strategy accumulates temporal changes into the token where the content first appears.

The same region may be represented at different spatial levels across frames, leading to two cases: many-to-one (fine-to-coarse) and one-to-many (coarse-to-fine). The many-to-one case is straightforward: merging fine tokens into a single coarse token in an early frame. The one-to-many case is complicated. Ideally, we would select the most similar fine-grained token as the destination, but this requires per-region comparisons that are difficult to vector-

ize and inefficient on GPUs. To address this, we approximate the merge direction by selecting the top-left token among candidates. This approximation allows us to implement temporal merging using a vectorized union-find algorithm [44], leading to efficient parallel processing.

Comprehensive experimental results across six video QA benchmarks demonstrate that our proposed method effectively reduces video tokens while maintaining high performance. As shown in Fig. 1, *STTM* outperforms both query-aware and query-agnostic methods overall. In the average results Fig. 1 (c, d), it achieves the highest accuracy with competitive latency under both 50% and 30% token budgets. A closer look at the per-dataset accuracy in Fig. 1 (a, b) further highlights its robustness, particularly on the challenging NIAH and long video datasets. Moreover, we validate *STTM*’s generalization by applying it to other LLMs and a large-scale 72B Video LLM.

## 2. Related Work

### 2.1. Spatio-Temporal Redundancy in Videos

Videos exhibit strong spatio-temporal locality – information within nearby regions in space and time is often redundant. This property has long been exploited across various domains. In deep learning, CNNs [18, 23] leverage spatial locality and are extended to 3D convolutions [4, 48] to model spatio-temporal correlations in video. In transformers, MAE [19] and VideoMAE [12, 46] show that reconstructing masked regions using local context is an effective self-supervised learning objective, implicitly benefiting from redundancy.

Similarity, video compression methods explicitly eliminate redundancy. Quadtree-based partitioning [13, 37] adapts block resolution based on regional complexity [41, 42, 52]. Temporal redundancy is also reduced, for example through the *Skip* mode in H.264/AVC [52], which omits re-encoding regions that remain unchanged across frames. Inspired by these principles, we propose a multi-granular spatio-temporal token merging method that explicitly compresses redundant video tokens by exploiting local similarity in both space and time.

### 2.2. Long Context Modeling in Video LLMs

In the early stages, LLMs had a limited maximum context length; for instance, LLaMA [47] supported only 2048 tokens. To handle extensive video context, multimodal LLMs integrate abstractor architectures [5, 24, 25] that reduce visual tokens before passing them into the language model. For video LLMs, Q-Former [25] based architecture has been widely adopted to reduce the number of visual tokens from a video [26–28, 32, 35, 36, 39, 51, 58], instead of using linear projectors, which preserve the original token count.

However, with the introduction of FlashAttention [9, 10],

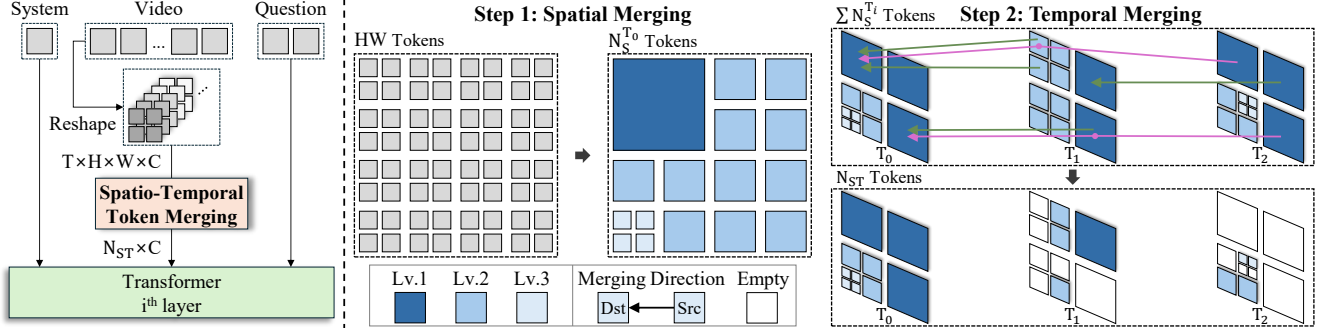


Figure 2. (Left) Our spatio-temporal token merging method is a training-free, plug-and-play module that produces spatio-temporally multi-granular tokens. (Middle) In step 1, tokens are merged based on spatial locality, where similar tokens within a 2D grid are combined into a single token. (Right) In step 2, spatially multi-granular tokens are further merged along the temporal dimension, where similar tokens across frames are consolidated into their earliest occurrence. The arrows indicate the direction of token merging. The green lines indicate merging over one timestep, and magenta lines are merging over two timesteps. The scale and the number of tokens are set for illustration.

which reduces the memory complexity of attention from quadratic to linear in sequence length, linear projector-based approaches have recently gained more attention and showed better performance than abstractor-based approaches. Furthermore, recent methods such as RingAttention [31] have enabled video LLMs [7, 30] to process up to one million video tokens. Following this trend, handling thousands of frames without downsampling is expected to become common in the future. However, such a large number of tokens significantly increases latency, highlighting the need for effective video token compression.

### 2.3. Training-Free Token Reduction in Video LLMs

Token reduction aims to identify and reduce highly redundant or less informative tokens, and has been researched in the architecture of Vision Transformer [2, 8]. Due to high computational costs in long video LLMs [7], studying token reduction in the regime of multimodal LLMs is being spotlighted [6, 15, 20, 21, 38, 43, 49, 55].

In the initial works [6, 38], visual tokens are reduced without considering the visual structure such as the 2D locality. One-dimensional token reduction methods treating visual tokens as a sequential stream, similar to text tokens, without considering spatial or temporal relationships. FastV [6] reduces low-rank visual tokens based on attention patterns in the early layers. Additionally, it employs text queries to search attention weights, requiring a token reduction to be performed again for each new query. In contrast, our method is query-agnostic, allowing KV cache reuse in LLMs, making it more efficient for conversational and multi-question scenarios.

Temporal token reduction methods exploit the redundancy between video frames. FrameFusion [15] demonstrates that the token similarity distribution condenses in deeper layers while preserving ranking consistency. It merges similar tokens between frames using similarity metrics and prunes unnecessary tokens based on attention scores. We argue that leveraging spatio-temporal character-

istics, rather than operating in a single dimension, enables more effective and efficient token reduction.

## 3. Methodology

We propose Spatio-Temporal Token Merging (STTM) that merges video tokens along spatial and temporal dimensions, producing multi-granular video tokens. This module is training-free and can be easily plugged into an intermediate layer of an LLM. As the STTM operates along the spatio-temporal dimension and outputs multi-granular tokens, it is designed as a single-pass operation, inserted into a single early layer of the transformer. Furthermore, our token reduction method is question-agnostic, enabling the reuse of KV caches across different questions for the same video.

### 3.1. Overview of STTM Module

As illustrated in Fig. 2, we use the video tokens from the previous layer’s output to perform token merging. After the merging process, the video tokens,  $Z_V \in \mathbb{R}^{T \times H \times W \times C}$ , are reduced into spatio-temporally merged tokens,  $Z_{ST} \in \mathbb{R}^{N_{ST} \times C}$ , where  $N_{ST} \ll T \times H \times W$ .

To exploit spatial locality, we first merge tokens that are similar within the 2D grid of each frame. As labeled by Lv.1, Lv.2, and Lv.3 in Fig. 2, we define the different scales of the 2D grid for merging unit. Based on these multi-scale merging grids, a large redundant region can be represented by a single coarse-grained token, achieving a high token reduction ratio. On the other hand, fine-grained tokens are used for representing the region with large variation. This spatial merging process results in spatially multi-granular tokens,  $Z_S^{T_i} \in \mathbb{R}^{N_S^{T_i} \times C}$ , where  $N_S^{T_i} \ll H \times W$ .

In videos, locality further extends to the spatio-temporal dimension. Thus, we merge tokens by comparing their similarities at the same 2D region across consecutive frames. When tokens remain similar over time, we chain them along a connected path and merge them into the earliest occurrence. Tokens with different spatial granularities can also be

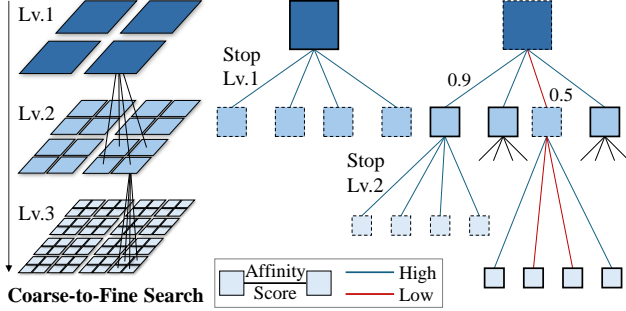


Figure 3. A **coarse-to-fine spatial search** is performed using a quadtree structure. If all four fine child nodes exhibit high similarity with the coarse parent node, the search process terminates, and the parent node is used to represent the corresponding region. Otherwise, the search continues until the finest level is reached. Here, the scale for each level is an example for illustration.

connected across frames when they overlap. As depicted in step 2 of Fig. 2, some fine-grained tokens at  $T_1$  are merged into a coarser token at  $T_0$ , while others remain separate due to low similarity. Our spatial and temporal hybrid merging allows multi-granular tokens in both dimensions.

### 3.2. Spatial Token Merging

As illustrated in Fig. 3, our approach employs a coarse-to-fine hierarchical search based on a quadtree data structure [13, 37]. At every level, each region requires only four comparisons for the *granularity decision process*; this process determines whether features at the current level sufficiently represent the region. If not, finer-grained features from the next level are adopted to represent the region without losing details. This hierarchical method effectively balances computational efficiency and representation flexibility. The quadtree structure organizes spatial tokens into a hierarchical representation, where each coarse-level parent node corresponds to four ( $2 \times 2$ ) finer-level child nodes within its respective 2D grid region. This hierarchical organization enables a structured approach to spatial token merging, preserving 2D locality, which is essential for subsequent temporal merging.

Building the quadtree follows three steps. First, we initialize leaf nodes of the quadtree based on the initial token feature map,  $Z_{lv}^{T_i} \in \mathbb{R}^{H \times W \times C}$ . Second, we construct a multi-scale representation by recursively downsampling the feature map until the feature map size reaches  $2 \times 2$ , which we denote as Lv.1, representing the coarsest spatial resolution. At each level, the feature map is downsampled by averaging spatially neighboring  $2 \times 2$  feature patches, yielding a coarser-level representation,  $Z_{lv-1}^{T_i} \in \mathbb{R}^{\frac{H}{2} \times \frac{W}{2} \times C}$ . During this downsampling operation, we connect four leaf nodes from  $Z_{lv}^{T_i}$  to a single parent node from  $Z_{lv-1}^{T_i}$ . Third, using this precomputed densely connected quadtree, we perform a quadtree search as described in Fig. 3 and keep only the necessary nodes to represent each frame.

For each level, we compute the cosine similarity between the current level’s nodes and their child nodes. When the similarities of four child nodes are higher than the spatial threshold value,  $\tau_S$ , we can regard this region has low spatial detail and terminate the further searching process for the corresponding node. As a result, all child nodes for this node are pruned in the quadtree. In contrast, when any of the child nodes show low similarity, we prune the current node and instead use the child nodes to represent the corresponding region. Thus, this quadtree search process can be regarded as the *granularity decision process*.

The computational complexity of our quadtree-based spatial merging algorithm follows  $\mathcal{O}(HW)$  per frame. The quadtree search is an iterative process that performs four comparisons for each node at a given level. In the worst case scenario, where all nodes are subdivided down to the deepest level, the computational cost of spatial token merging,  $C_{STM}$ , is the geometric series following:

$$C_{STM} = \sum_{i=1}^{Lv} \frac{HW}{4^i} \times 4 \quad (1)$$

Asymptotically,  $C_{STM}$  is bounded by the sum of infinite geometric series:

$$\lim_{Lv \rightarrow \infty} C_{STM} = \frac{HW}{1 - \frac{1}{4}} = \frac{4HW}{3} \quad (2)$$

Notably, we implement the quadtree search algorithm in parallel at each level, ensuring that the actual running time remains linear in complexity.

### 3.3. Temporal Token Merging

To capture the spatio-temporal redundancy, we compute the similarity of tokens representing the same region in neighboring two frames and make the connection between pairs of tokens exhibiting similarity higher than  $\tau_T$ . As we merge into the earlier tokens, this process results in directed graphs, where the source node is from  $T + 1$ , and the destination node is at  $T$ . Based on these directed graphs built from consecutive frames, we obtain connected graphs and identify the common root node for all nodes in the connected graph. The common root node and other nodes are set as destination and source, respectively, for merging. So, the nodes can be merged not only in consecutive two-frame sequences but also in the far distance. As shown in Fig. 2 (right), a token representing the top-left token at  $T_2$  is merged into the token at  $T_0$ , while the top-right token at  $T_2$  is merged into the token at  $T_1$ . This merging process results in spatio-temporally multi-scale tokens.

Since spatial merging results in varying scales of tokens, we cannot directly merge the tokens at the same exact spatial location across frames. Instead, we merge the tokens under their spatio-temporally overlapping regions. For example, in Fig. 2 step 2, top-left region is expressed in varying scales across frames. We compare the similarity be-

Token Budget	Method	Q. Agn.	VNBench			VideoMME			LongVideoBench			MLVU			EgoSchema			NExT-QA			Avg.		
			Acc ↑	TTFT ↓	N <sub>V</sub> ↓	Acc ↑	TTFT ↓	N <sub>V</sub> ↓	Acc ↑	TTFT ↓	N <sub>V</sub> ↓	Acc ↑	TTFT ↓	N <sub>V</sub> ↓	Acc ↑	TTFT ↓	N <sub>V</sub> ↓	Acc ↑	TTFT ↓	N <sub>V</sub> ↓	Acc ↑	TTFT ↓	N <sub>V</sub> ↓
100%	LLaVA-Video 7B	✓	77.6	0.962	11149	63.1	2.039	22086	59.6	1.805	19624	70.9	2.343	25088	58.7	2.312	25069	82.9	0.659	8116	n.a	n.a	n.a
50%	+ FastV		93.7	52.3	50.0	96.7	50.7	50.0	96.2	50.8	50.0	96.4	49.7	50.0	98.2	50.4	50.0	99.3	53.5	50.0	96.8	51.2	50.0
	+ DyCoke		92.9	47.6	49.4	97.4	44.7	47.9	97.5	45.4	48.5	98.1	44.7	47.7	99.9	45.4	47.7	99.0	50.0	49.3	97.5	46.3	48.4
	+ FrameFusion		98.2	49.0	49.4	98.3	47.1	48.7	99.4	47.2	49.1	97.9	46.3	48.4	98.4	47.0	49.1	99.6	50.9	49.6	98.6	47.9	49.0
	+ ToMe	✓	95.5	53.8	50.0	97.4	51.1	50.0	97.4	52.6	50.0	98.4	50.9	50.0	100.1	51.9	50.0	99.6	56.1	50.0	98.1	52.7	50.0
	+ DyCoke-stage1	✓	94.4	51.4	49.4	98.2	48.1	47.9	97.6	48.6	48.5	98.4	47.9	47.7	100.1	48.4	47.7	99.3	53.0	49.3	98.0	49.6	48.4
	+ STTM (Ours)	✓	99.8	47.3	45.5	99.2	50.1	47.1	100.0	49.6	45.6	98.6	49.2	48.6	99.9	45.2	42.8	99.5	48.9	43.7	99.5	48.4	45.5
30%	+ FastV		79.3	34.9	30.0	93.8	33.5	30.0	91.8	33.8	30.0	94.5	32.7	30.0	97.1	33.4	30.0	98.4	36.4	30.0	92.5	34.1	30.0
	+ DyCoke		72.0	32.0	33.0	96.2	29.3	31.2	95.9	30.2	32.1	95.0	29.2	31.1	99.4	30.0	31.1	98.3	34.7	33.2	92.8	30.9	31.9
	+ FrameFusion		93.3	30.3	28.1	96.2	28.5	27.4	95.7	28.8	27.9	95.2	27.8	27.0	97.8	28.4	27.4	98.8	33.0	28.4	96.2	29.5	27.7
	+ ToMe	✓	82.7	37.8	30.0	93.8	35.3	30.0	94.5	36.5	30.0	94.5	35.0	30.0	97.9	36.1	30.0	98.4	40.2	30.0	93.6	36.8	30.0
	+ DyCoke-stage1	✓	82.3	37.2	33.3	95.0	34.3	31.2	94.9	35.0	32.1	96.8	34.0	31.1	100.0	34.6	31.1	98.5	38.9	33.2	94.6	35.7	32.0
	+ STTM (Ours)	✓	98.0	31.1	25.8	98.8	31.4	25.8	95.6	34.1	28.3	96.7	32.8	29.2	98.9	33.4	29.1	98.9	35.7	27.3	97.8	33.1	27.6

Table 1. Comparison of training-free token reduction methods using LLaVA-Video-7B under 50% and 30% pre-filling token budgets. Token-reduced results are reported relative to the result with 100% .

tween a single Lv.1 token at  $T_0$  and  $2 \times 2$  Lv.2 tokens at  $T_1$ . Two Lv.2 tokens at  $T_1$  with high similarity are merged into the token at  $T_0$ , while the other two remain to represent a change in  $T_1$ 's top-left region.

During temporal merging, we set the direction of merging as tokens at the earlier frame. In the case of top-left at  $T_1$  and  $T_2$ , the token at  $T_2$  is coarser than  $T_1$  and has four possible destination paths for merging. When there are multiple connections with similarity higher than  $\tau_T$ , we provide the priority to the token located towards top-left. We simplify the choice of choosing the top-left merging token for such multiple destination cases primarily for parallel indexing implementation, although merging with the most similar token is the naive method.

The computational complexity of our temporal merging algorithm follows  $\mathcal{O}(THW)$  per video. Suppose the worst case is that spatial tokens of all frames are in the finest level, incurring  $(T - 1) \times H \times W$  comparisons. However, we can expect more efficiency gain since spatial merging results in fewer tokens at every frame, reducing the comparisons. Computing the common root node can also be achieved in  $\mathcal{O}(THW)$  by adapting the union-find algorithm [44] into a vectorized form.

### 3.4. Token Reordering after Merging

After spatio-temporal token merging, the resulting video tokens form a graph structure. To serve as input for an LLM, this graph must be linearized into a one-dimensional sequence. In our reordering strategy, we prioritize tokens based on two criteria. First, spatial ordering follows a Z-shaped scan based on each token's top-left coordinate. Second, temporal ordering gives precedence to tokens from earlier frames over those from later ones.

Once reordered into a 1D sequence, handling positional embeddings becomes crucial. Recent LLMs typically use rotary positional embeddings (RoPE) [40], which apply a rotation matrix computed from each token's position index. We evaluate three strategies for assigning RoPE after merging: (1) Merged RoPE, which averages the RoPEs of

merged tokens; (2) Survived RoPE, which retains the original RoPEs of the surviving tokens; (3) Reassigned RoPE, which reassigns position IDs based on the new token order for alignment with the original positional encoding.

## 4. Experiments

### 4.1. Evaluation Setting

**Datasets.** To focus on visual understanding, we adopt an evaluation setting without subtitles. We evaluate methods on six diverse video QA benchmarks. These include short-form datasets, EgoSchema [33] and NExT-QA [54], as well as long-form datasets with hour-long videos: VideoMME [14], LongVideoBench [53], and MLVU [62]. To rigorously evaluate fine-grained spatio-temporal understanding, we use VNBench [61], a synthetic dataset simulating the *needle in a haystack* task [22]. It introduces subtle visual or textual "needles" into short segments of a video – irrelevant to the original content but relevant to the question. **Evaluation Metrics.** We report standard accuracy for multiple-choice question answering. For practicality, we include the average running time (in seconds) and the number of visual tokens ( $N_V$ ). Since our focus is on the pre-filling stage, we measure the time-to-first-token (TTFT). In addition to absolute values, we provide relative values (R.) with respect to performance without token reduction.

**Implementation Details.** We sample video frames at 1 FPS, but uniformly sample frames if a video exceeds the maximum frame limit. To ensure coverage of injected needles in VNBench, we set the maximum number of frames to 180; for other datasets, we use a limit of 128 frames. A single and four A100 80G GPUs are used for 7B and 72B models, respectively. Our merging threshold values ( $\tau_S$  and  $\tau_T$ ) are empirically adjusted to approximately meet specific token budget for fair comparisons with other methods.

### 4.2. Comparison with Existing Methods

We compare other methods [2, 6, 15, 43] under the same experimental setup. ToMe [2] is applied within an LLM rather than its original ViT-based setting. DyCoke-stage1 refers to

Token Budget	Method	Q. Agn.	VNBench			VideoMME			LongVideoBench			MLVU			EgoSchema			NExT-QA			Avg.		
			Acc ↑	TTFT ↓	N <sub>V</sub> ↓	Acc ↑	TTFT ↓	N <sub>V</sub> ↓	Acc ↑	TTFT ↓	N <sub>V</sub> ↓	Acc ↑	TTFT ↓	N <sub>V</sub> ↓	Acc ↑	TTFT ↓	N <sub>V</sub> ↓	Acc ↑	TTFT ↓	N <sub>V</sub> ↓	Acc ↑	TTFT ↓	N <sub>V</sub> ↓
100%	<i>LLaVA-OV 7B</i>	✓	68.8	0.922	11149	59.0	1.904	22086	56.3	1.712	19624	67.5	2.224	25088	61.3	2.216	25069	80.6	0.630	8116	n/a	n/a	n/a
50%	+ FastV		95.3	50.7	50.0	99.0	49.1	50.0	99.7	49.2	50.0	99.9	48.1	50.0	99.4	48.8	50.0	99.5	52.3	50.0	98.8	49.7	50.0
	+ DyCoke		94.3	45.3	49.4	101.8	43.7	47.9	102.8	43.2	48.5	101.8	42.3	47.7	100.8	42.8	47.7	99.7	47.8	49.3	100.2	44.2	48.4
	+ FrameFusion		98.6	47.2	49.8	101.4	45.4	49.4	100.5	45.5	49.6	101.0	44.7	49.3	99.1	45.0	49.9	100.2	49.5	50.0	100.1	46.2	49.7
	+ ToMe	✓	97.5	52.4	50.0	101.4	50.6	50.0	102.5	50.5	50.0	102.0	49.5	50.0	101.6	50.0	50.0	99.4	54.4	50.0	100.7	51.2	50.5
	+ DyCoke-stage1	✓	94.6	49.7	49.4	100.6	47.9	47.9	103.3	48.0	48.5	102.5	46.7	47.7	100.8	47.3	47.7	100.0	51.8	49.3	100.3	48.6	48.4
	+ STTM (Ours)	✓	103.6	43.8	44.2	102.8	40.6	37.5	102.4	47.0	44.6	103.3	45.9	46.6	100.6	43.9	43.6	99.8	49.5	46.4	<b>102.1</b>	<b>45.1</b>	<b>43.8</b>
30%	+ FastV		86.1	32.8	30.0	98.6	31.4	30.0	98.1	31.7	30.0	97.2	30.6	30.0	99.3	31.3	30.0	98.8	34.6	30.0	96.4	32.1	30.0
	+ DyCoke		78.4	30.3	33.3	101.4	28.2	31.2	99.3	28.5	32.1	101.2	26.9	31.1	101.2	27.4	31.1	98.9	33.0	33.2	96.7	29.1	32.0
	+ FrameFusion		96.0	28.3	29.0	100.1	26.2	28.0	100.4	26.6	28.5	98.8	25.6	27.6	98.3	26.3	28.9	99.1	31.0	29.5	98.8	27.3	28.6
	+ ToMe	✓	86.0	36.0	30.0	101.4	34.1	30.0	100.3	34.3	30.0	102.4	33.3	30.0	101.3	33.8	30.0	98.6	38.1	30.0	98.3	34.9	30.0
	+ DyCoke-stage1	✓	84.9	35.1	33.3	102.3	33.2	31.2	99.7	33.7	32.1	100.7	32.5	31.1	101.5	33.0	31.1	98.8	37.4	33.2	98.0	34.2	32.0
	+ STTM (Ours)	✓	102.3	30.1	27.4	102.6	31.6	27.3	100.5	33.3	30.0	101.4	33.0	31.8	100.7	25.7	22.4	98.9	38.1	33.1	<b>101.1</b>	<b>32.0</b>	<b>28.7</b>

Table 2. Comparison of training-free token reduction methods using LLaVA-OneVision-7B. Relative to 100% result .

Token Budget	Method	VNBench			VideoMME			LongVideoBench			Avg.		
		Acc ↑	TTFT ↓	N <sub>V</sub> ↓	Acc ↑	TTFT ↓	N <sub>V</sub> ↓	Acc ↑	TTFT ↓	N <sub>V</sub> ↓	Acc ↑	TTFT ↓	N <sub>V</sub> ↓
100%	<i>Qwen2VL 7B</i>	66.4	2.438	22025	61.8	10.745	74982	56.8	10.597	72109	n.a	n.a	n.a
50%	+ ToMe	95.5	46.3	50.0	100.1	42.0	50.0	101.4	41.9	50.0	99.0	43.4	50.0
	+ DyCoke-stage1	98.1	43.0	49.6	101.2	38.8	48.1	101.2	39.1	48.8	100.2	40.3	<b>48.8</b>
	+ STTM (Ours)	105.2	29.8	48.9	101.8	44.3	52.3	101.1	43.5	51.5	<b>102.7</b>	<b>39.2</b>	50.9
30%	+ ToMe	85.6	30.3	30.0	99.3	26.4	30.0	99.5	26.3	30.0	94.8	27.7	<b>30.0</b>
	+ DyCoke-stage1	81.6	29.0	33.4	99.9	25.2	31.4	101.2	25.4	32.3	94.2	26.5	32.4
	+ STTM (Ours)	100.4	17.2	30.6	101.0	25.7	32.9	100.1	23.3	27.7	<b>100.5</b>	<b>22.1</b>	30.4

Table 3. Comparison using Qwen2VL-7B. Relative to 100% result .

Token Budget	Method	VideoMME		
		Acc ↑	TTFT ↓	N <sub>V</sub> ↓
100%	<i>LLaVA-Video 72B</i>	70.5	17.698	22086
50%	+ ToMe	100.1	47.6	50.0
	+ DyCoke-stage1	99.8	45.5	47.9
	+ STTM (Ours)	<b>101.3</b>	<b>44.2</b>	<b>44.2</b>
30%	+ ToMe	97.1	<b>29.3</b>	<b>30.0</b>
	+ DyCoke-stage1	98.3	30.2	31.2
	+ STTM (Ours)	<b>99.1</b>	30.5	30.5

Table 4. Comparison using LLaVA-Video-72B. Relative to 100% result .

a technique for pre-filling stage [43]. We report relative values here, with absolute values provided in Appendix.

**Performance of LLaVA-Video-7B.** Our method outperforms both query-aware and query-agnostic methods on average across benchmarks (Tab. 1). On **average**, it incurs only 0.5% and 2.2% relative accuracy drops under the 50% and 30% budgets, respectively. On **VNBench** (30% budget), other Q.Agn methods exhibit large drops (about 18%), but it shows only a 2.0% drop. These results indicate that our method better preserves fine-grained spatio-temporal details. All methods apply token reduction with  $\mathcal{O}(N)$  complexity; thus, TTFT is dominated by attention in the LLM layers and scales with the number of retained tokens. Since tokens are reduced at the input or in the early LLM layers, all methods exhibit similar TTFT at each token budget.

**Generalization to Other MLLMs.** We also evaluate our method with LLaVA-OneVision (Tab. 2) and Qwen2VL (Tab. 3), and it continues to outperform other methods on both MLLMs. Notably, it even improves accuracy while using fewer tokens (under both 50% and 30% budgets). We observe accuracy improvements of 1.1% and 0.5%, along with  $3.1\times$  and  $4.5\times$  speed-ups, for OneVision and Qwen2VL, respectively. Qwen2VL consumes more visual tokens than LLaVA-based models, resulting in a greater latency reduction due to the quadratic complexity of attention.

**Scaling to 72B.** Our method continues to outperform other methods on the 72B LLM under both 50% and 30% token budgets (Tab. 4). Notably, it even improves accuracy by 1.3% while using only 44.2% of the tokens. The 72B model requires substantial processing time per request (e.g., an average of 17.7 seconds). As a query-agnostic method,

it performs token reduction without relying on the question, enabling reuse of the KV cache for the same video across different questions. This improves deployment efficiency in multi-turn or multi-query scenarios.

### 4.3. Ablation Study

We conduct ablation studies to validate effectiveness of the proposed components using LLaVA-Video-7B.

**Multi-Granularity Spatial Tokens.** To evaluate the effectiveness of our hierarchical spatial token merging method, we compare it against a single-granularity method using bilinear interpolation (Tab. 5). On VideoMME, the single-granularity method performs competitively, even surpassing FastV [6] while using only 41.3% of the tokens. However, its accuracy drops significantly on VNBench which requires fine-grained spatial information. In contrast, our quadtree-based multi-granularity merging maintains accuracy across both datasets. At  $\tau_S$  of 0.80, it incurs only 1.3% and 0.8% drop in relative accuracy with a token budget of approximately 50%. This highlights the advantage of incorporating multi-granularity spatial tokens for balancing compression efficiency and accuracy retention.

**Root Node Spatial Resolution.** As shown in Tab. 5, using a coarser spatial scale ( $2\times 2$ ) for root node initialization leads to a lower relative  $N_V$  at the same spatial threshold. This indicates that more tokens are merged and each frame is represented by coarser spatial tokens. However, this higher compression ratio comes at the cost of a significant accuracy drop compared to using root nodes with a  $4\times 4$  spatial scale. The effect is particularly pronounced at lower  $\tau_S$ , where the accuracy degradation is more severe,

Token Granularity	Lv.1 Scale	$\tau_S$	VNBench		VideoMME	
			R.Acc $\uparrow$	R.N <sub>V</sub> $\downarrow$	R.Acc $\uparrow$	R.N <sub>V</sub> $\downarrow$
Single	13×13		82.1	86.2	99.2	86.2
Multi	2×2	0.85	88.1	54.2	98.1	58.2
Multi	4×4	0.85	99.9	82.0	99.5	83.0
Single	11×11		80.0	61.7	98.4	61.7
Multi	2×2	0.80	73.1	27.0	96.2	31.5
Multi	4×4	0.80	98.7	57.2	99.2	59.9
Single	9×9		78.9	41.3	97.4	41.3
Multi	2×2	0.75	62.6	13.3	92.5	15.8
Multi	4×4	0.75	93.0	35.8	97.5	38.9
FastV			93.7	50.0	96.7	50.0

Table 5. Ablation study on the proposed multi-granular spatial token merging. Lv.1: spatial scale of root nodes.

LLM Layer	VNBench			VideoMME		
	R.Acc $\uparrow$	R.TTFT $\downarrow$	R.N <sub>V</sub> $\downarrow$	R.Acc $\uparrow$	R.TTFT $\downarrow$	R.N <sub>V</sub> $\downarrow$
1	95.8	<b>27.9</b>	28.3	96.0	<b>26.5</b>	26.4
3	98.0	30.9	25.8	98.8	31.3	25.8
7	98.2	40.6	<b>24.8</b>	97.9	41.6	25.6
19	<b>99.5</b>	75.5	31.7	<b>99.2</b>	71.6	<b>22.6</b>

Table 9. Ablation study of token merging position.

G-Token	VNB	VidMME	LVB	MLVU	EgoS	NEXt	Avg. ( $\Delta$ )
✓	<b>78.2</b>	62.6	58.9	70.6	58.5	82.2	68.5
✗	77.6	<b>63.1</b>	<b>59.6</b>	<b>70.9</b>	<b>58.7</b>	<b>82.9</b>	<b>68.8 (+0.3)</b>

Table 10. Effect of grid token removal on accuracy.

especially on VNBench. This is due to the loss of spatial details, as quadtree subdivision from a  $2 \times 2$  root may terminate prematurely, producing tokens that are too coarse to retain essential visual information. To address this, we adopt a  $4 \times 4$  spatial scale for root nodes, which enables lower  $\tau_S$  for higher compression while preserving accuracy.

**Decomposed Spatio-Temporal Merging.** In our algorithm, we first perform spatial merging, followed by temporal merging in sequence. Tab. 6 presents the impact of spatial and temporal merging, individually. While both methods effectively reduce the number of tokens, applying them sequentially yields a synergistic effect, achieving a high token reduction ratio with only a marginal accuracy drop. Additionally, we experiment with a joint spatio-temporal merging method based on an octree data structure, which partitions a long video into predefined cubic segments and recursively subdivides them at a  $2 \times 2 \times 2$  finer scale. While this method shows promising results on VideoMME, it leads to a significant accuracy drop on VNBench, where rapid spatial changes occur within short time intervals. This suggests that rigid hierarchical partitioning across spatio-temporal dimensions is not effective in dynamic scenarios. Therefore, we adopt a decomposed merging strategy.

**Approximated Temporal Matching.** As shown in Tab. 7, selecting the most similar destination node does not consistently improve performance. In contrast, using a top-left approximation enables a vectorized union-find algorithm [44], avoiding costly similarity checks, and leads to significant runtime improvement without drop in accuracy.

**Positional Embedding.** Tab. 8 shows the results of dif-

STM	TTM	VNBench		VideoMME	
		R.Acc. $\uparrow$	R.N <sub>V</sub> $\downarrow$	R.Acc. $\uparrow$	R.N <sub>V</sub> $\downarrow$
✓	✗	98.7	57.2	99.2	59.9
✗	✓	100.0	53.7	99.9	56.7
✓	✓	98.0	25.8	98.8	25.8
✓	✓	73.3	27.0	95.5	32.0

Table 6. Effectiveness of spatial and temporal merging modules. Sequentially combining these two modules results in a synergistic effect. Last row: joint merging.

Method	R.Acc $\uparrow$	R.TTFT $\downarrow$	R.N <sub>V</sub> $\downarrow$
Optimal	<b>99.6</b>	58.1	47.7
Top-left	99.2	<b>50.1</b>	<b>47.1</b>
Optimal	97.7	39.6	27.7
Top-left	<b>98.8</b>	<b>31.4</b>	<b>25.8</b>

Table 7. Temporal merging ablation

Positional Embedding	VNB	VidMME
	R.Acc $\uparrow$	R.Acc $\uparrow$
Merging	96.0	95.7
Survival	96.5	96.0
Reassignment	<b>98.0</b>	<b>98.8</b>

Table 8. Ablation study on positional embedding after merging.

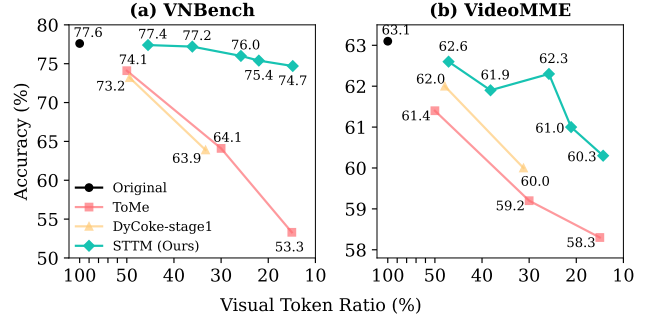


Figure 4. Trade-off of accuracy and visual token retention ratio.

ferent strategies for handling positional embeddings during token merging within LLM layers. We observe that preserving the original positional embeddings yields better performance than merging them. Since Qwen2VL [50] uses M-RoPE, which computes positions based on (t, y, x), we cannot apply the reassignment strategy and instead adopt the survival strategy.

**Merging Layer Position.** We evaluate the impact of different LLM layer positions for video token merging (Tab. 9). As observed in recent works [3, 6, 55, 57], performing token merging at later layers yields higher accuracy but lower speed-up, due to increased full-token attention computations. Merging tokens before the third LLM layer provides a good trade-off between accuracy and latency; we adopt this configuration for 7B models, while for the 72B model, we merge tokens before the first LLM layer.

**Grid Token.** As shown in Tab. 10, removing the special grid token used for video data in LLaVA-Video does not degrade accuracy across benchmarks. To simplify the handling of video tokens during spatio-temporal merging, we omit such token in LLaVA-Video and OneVision.

**Accuracy vs. Compression.** Fig. 4 illustrates the trade-off between accuracy and visual token retention ratio. On both datasets, our method consistently outperforms other query-agnostic token reduction methods [2, 43] across token retention levels, ranging from 50% to 15%. This demonstrates the robustness of our method in achieving a favorable balance between compression efficiency and accuracy.

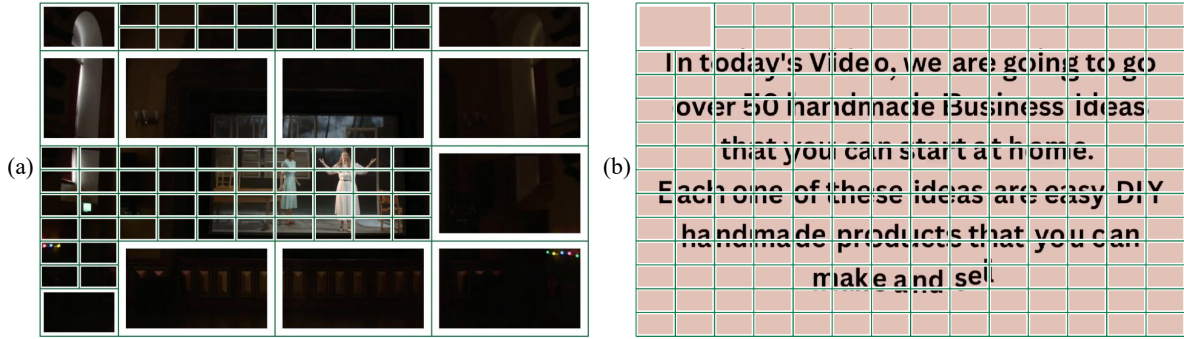


Figure 5. Visualization of spatial token merging results. Each image patch within a green box represents a single token.

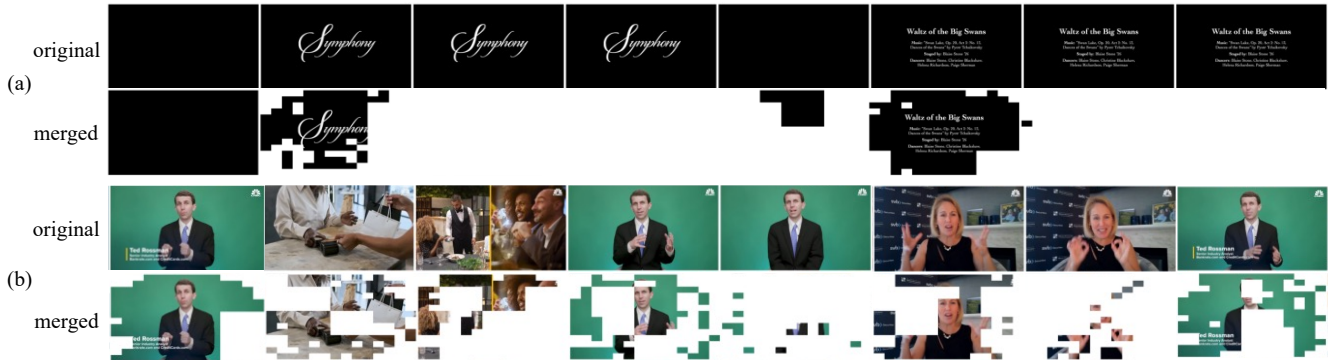


Figure 6. Visualization of spatio-temporal token merging results on VideoMME. (a) The first eight consecutive frames are sampled. (b) Intermediate frames are sampled for illustration purpose. Empty regions indicate areas that have been merged with early tokens.

#### 4.4. Visualization of Token Merging

Unlike uniform reduction methods, STTM adaptively reduces tokens based on the redundancy present in each video. It allocates more tokens to regions that require fine-grained detail, while aggressively reducing tokens in redundant areas. On VideoMME (30% budget), its token retention ranges from 3.3% to 51.2% across videos, demonstrating its adaptability to varying content complexity.

Fig. 5 presents the results of spatial merging before applying temporal merging. Fig. 5 (a) illustrates a case where semantically similar tokens are effectively merged, reducing 196 visual tokens to 63 in a frame. In contrast, Fig. 6 (b) shows a worst-case scenario for spatial compression. In this frame, fine-grained tokens are preserved to retain small text details. Although the compression rate is low, OCR accuracy on VideoMME is maintained after token merging. While using all tokens yields an OCR accuracy of 67.6, ToMe, DyCoke-stage1, and our method achieve 58.3, 64.7, and 65.5, respectively, under token reduction.

Fig. 6 shows the results of spatio-temporal merging. In Fig. 6 (a), regions with newly emerging content remain intact, while redundant regions across consecutive frames are merged. For instance, letter regions that appear in the second and sixth frames are preserved, while background tokens, such as the black areas, are merged into the earlier frames. Duplicated frames (e.g., frames 3, 4, 7, and 8) are

almost entirely merged. Fig. 6 (b) illustrates an example with dynamic scene changes. Similarly, within each scene, later frames tend to be merged into the first frame of the segment (e.g., frames 4 and 5). Notably, subtle but semantically meaningful changes – such as facial expressions or hand gestures – are preserved in frames 6 and 7.

#### 5. Conclusion

This is the first work to explore multi-granular video token merging in a training-free manner for video LLMs. We propose a decomposed spatio-temporal token merging method, called STTM. Its effectiveness is validated across six video QA benchmarks. Notably, it largely outperforms others on VNBench which requires fine-grained understanding. Since our method operates independently of user instructions, the KV cache can be reused across different questions for the same video, improving computational efficiency. While our method successfully minimizes spatio-temporal redundancy, its performance currently depends on manually adjusted threshold values. Exploring adaptive threshold selection is a promising direction, enabling automatic adjustment of token merging based on the given token budget.

**Acknowledgements.** This work was partly supported by the NAVER Cloud Corporation.

## References

- [1] Jinze Bai, Shuai Bai, Shusheng Yang, Shijie Wang, Sinan Tan, Peng Wang, Junyang Lin, Chang Zhou, and Jingren Zhou. Qwen-vl: A frontier large vision-language model with versatile abilities. *arXiv preprint arXiv:2308.12966*, 2023. 1
- [2] Daniel Bolya, Cheng-Yang Fu, Xiaoqi Dai, Peizhao Zhang, Christoph Feichtenhofer, and Judy Hoffman. Token merging: Your vit but faster. In *ICLR*, 2023. 3, 5, 7
- [3] Zefan Cai, Yichi Zhang, Bofei Gao, Yuliang Liu, Tianyu Liu, Keming Lu, Wayne Xiong, Yue Dong, Baobao Chang, Junjie Hu, et al. Pyramidkv: Dynamic kv cache compression based on pyramidal information funneling. *arXiv preprint arXiv:2406.02069*, 2024. 7
- [4] Joao Carreira and Andrew Zisserman. Quo vadis, action recognition? a new model and the kinetics dataset. In *CVPR*, pages 6299–6308, 2017. 2
- [5] Junbum Cha, Wooyoung Kang, Jonghwan Mun, and Byungseok Roh. Honeybee: Locality-enhanced projector for multimodal llm. In *CVPR*, pages 13817–13827, 2024. 2
- [6] Liang Chen, Haozhe Zhao, Tianyu Liu, Shuai Bai, Junyang Lin, Chang Zhou, and Baobao Chang. An image is worth 1/2 tokens after layer 2: Plug-and-play inference acceleration for large vision-language models. In *ECCV*, pages 19–35. Springer, 2024. 2, 3, 5, 6, 7
- [7] Yukang Chen, Fuzhao Xue, Dacheng Li, Qinghao Hu, Ligeng Zhu, Xiuyu Li, Yunhao Fang, Haotian Tang, Shang Yang, Zhijian Liu, Yihui He, Hongxu Yin, Pavlo Molchanov, Jan Kautz, Linxi Fan, Yuke Zhu, Yao Lu, and Song Han. Longvila: Scaling long-context visual language models for long videos. In *ICLR*, 2025. 1, 3
- [8] Joonmyung Choi, Sanghyeok Lee, Jaewon Chu, Minhyuk Choi, and Hyunwoo J Kim. vid-tldr: Training free token merging for light-weight video transformer. In *CVPR*, pages 18771–18781, 2024. 3
- [9] Tri Dao. FlashAttention-2: Faster attention with better parallelism and work partitioning. In *ICLR*, 2024. 1, 2
- [10] Tri Dao, Daniel Y. Fu, Stefano Ermon, Atri Rudra, and Christopher Ré. FlashAttention: Fast and memory-efficient exact attention with IO-awareness. In *NeurIPS*, 2022. 1, 2
- [11] Abhimanyu Dubey, Abhinav Jauhri, Abhinav Pandey, Abhishek Kadian, Ahmad Al-Dahle, Aiesha Letman, Akhil Mathur, Alan Schelten, Amy Yang, Angela Fan, et al. The llama 3 herd of models. *arXiv preprint arXiv:2407.21783*, 2024. 1
- [12] Christoph Feichtenhofer, Yanghao Li, Kaiming He, et al. Masked autoencoders as spatiotemporal learners. *NeurIPS*, 35:35946–35958, 2022. 2
- [13] Raphael A Finkel and Jon Louis Bentley. Quad trees a data structure for retrieval on composite keys. *Acta informatica*, 4:1–9, 1974. 2, 4
- [14] Chaoyou Fu, Yuhan Dai, Yongdong Luo, Lei Li, Shuhuai Ren, Renrui Zhang, Zihan Wang, Chenyu Zhou, Yunhang Shen, Mengdan Zhang, et al. Video-mme: The first-ever comprehensive evaluation benchmark of multi-modal llms in video analysis. In *CVPR*, pages 24108–24118, 2025. 5
- [15] Tianyu Fu, Tengxuan Liu, Qinghao Han, Guohao Dai, Shengen Yan, Huazhong Yang, Xuefei Ning, and Yu Wang. Framefusion: Combining similarity and importance for video token reduction on large visual language models. *arXiv preprint arXiv:2501.01986*, 2024. 2, 3, 5
- [16] Google. Caching — google ai, 2024. Accessed: 2025-07-09. 1
- [17] Gemini Team Google. Gemini 1.5: Unlocking multimodal understanding across millions of tokens of context. *arXiv preprint arXiv:2403.05530*, 2024. 1
- [18] Kaiming He, Xiangyu Zhang, Shaoqing Ren, and Jian Sun. Deep residual learning for image recognition. In *CVPR*, pages 770–778, 2016. 2
- [19] Kaiming He, Xinlei Chen, Saining Xie, Yanghao Li, Piotr Dollár, and Ross Girshick. Masked autoencoders are scalable vision learners. In *CVPR*, pages 16000–16009, 2022. 2
- [20] Xiaohu Huang, Hao Zhou, and Kai Han. Prunevid: Visual token pruning for efficient video large language models. *arXiv preprint arXiv:2412.16117*, 2024. 2, 3
- [21] Peng Jin, Ryuichi Takanobu, Wancai Zhang, Xiaochun Cao, and Li Yuan. Chat-univi: Unified visual representation empowers large language models with image and video understanding. In *CVPR*, pages 13700–13710, 2024. 3
- [22] G Kamradt. Needle in a haystack – pressure testing llms. [https://github.com/gkamradt/LLMTest\\_NeedleInAHaystack](https://github.com/gkamradt/LLMTest_NeedleInAHaystack), 2023. 5
- [23] Yann LeCun, Bernhard Boser, John Denker, Donnie Henderson, Richard Howard, Wayne Hubbard, and Lawrence Jackel. Handwritten digit recognition with a back-propagation network. *NeurIPS*, 2, 1989. 2
- [24] Junnan Li, Dongxu Li, Caiming Xiong, and Steven Hoi. Blip: Bootstrapping language-image pre-training for unified vision-language understanding and generation. In *ICML*, pages 12888–12900. PMLR, 2022. 2
- [25] Junnan Li, Dongxu Li, Silvio Savarese, and Steven Hoi. Blip-2: Bootstrapping language-image pre-training with frozen image encoders and large language models. In *ICML*, pages 19730–19742. PMLR, 2023. 1, 2
- [26] KunChang Li, Yanan He, Yi Wang, Yizhuo Li, Wenhai Wang, Ping Luo, Yali Wang, Limin Wang, and Yu Qiao. Videochat: Chat-centric video understanding. *arXiv preprint arXiv:2305.06355*, 2023. 1, 2
- [27] Kunchang Li, Yali Wang, Yanan He, Yizhuo Li, Yi Wang, Yi Liu, Zun Wang, Jilan Xu, Guo Chen, Ping Luo, Limin Wang, and Yu Qiao. Mvbench: A comprehensive multi-modal video understanding benchmark. In *CVPR*, pages 22195–22206, 2024. 1
- [28] Bin Lin, Yang Ye, Bin Zhu, Jiayi Cui, Munan Ning, Peng Jin, and Li Yuan. Video-llava: Learning united visual representation by alignment before projection. In *EMNLP*, 2024. 2
- [29] Haotian Liu, Chunyuan Li, Qingyang Wu, and Yong Jae Lee. Visual instruction tuning. *NeurIPS*, 36, 2023. 1
- [30] Hao Liu, Wilson Yan, Matei Zaharia, and Pieter Abbeel. World model on million-length video and language with blockwise ringattention. *arXiv preprint arXiv:2402.08268*, 2024. 1, 3
- [31] Hao Liu, Matei Zaharia, and Pieter Abbeel. Ring attention with blockwise transformers for near-infinite context. In *ICLR*, 2024. 1, 3

- [32] Muhammad Maaz, Hanoona Rasheed, Salman Khan, and Fahad Shahbaz Khan. Video-chatgpt: Towards detailed video understanding via large vision and language models. In *ACL*, 2024. 1, 2
- [33] Karttikeya Mangalam, Raiymbek Akshulakov, and Jitendra Malik. Egoschema: A diagnostic benchmark for very long-form video language understanding. *NeurIPS*, 36:46212–46244, 2023. 5
- [34] Reiner Pope, Sholto Douglas, Aakanksha Chowdhery, Jacob Devlin, James Bradbury, Jonathan Heek, Kefan Xiao, Shivani Agrawal, and Jeff Dean. Efficiently scaling transformer inference. *MLSys*, 5:606–624, 2023. 1
- [35] Shuhuai Ren, Linli Yao, Shicheng Li, Xu Sun, and Lu Hou. Timechat: A time-sensitive multimodal large language model for long video understanding. In *CVPR*, pages 14313–14323, 2024. 1, 2
- [36] Michael S Ryoo, Honglu Zhou, Shrikant Kendre, Can Qin, Le Xue, Manli Shu, Silvio Savarese, Ran Xu, Caiming Xiong, and Juan Carlos Niebles. xgen-mm-vid (blip-3-video): You only need 32 tokens to represent a video even in vlms. *arXiv preprint arXiv:2410.16267*, 2024. 2
- [37] Hanan Samet. The quadtree and related hierarchical data structures. *ACM CSUR*, 16(2):187–260, 1984. 2, 4
- [38] Yuzhang Shang, Mu Cai, Bingxin Xu, Yong Jae Lee, and Yan Yan. Llava-prumerge: Adaptive token reduction for efficient large multimodal models. *arXiv preprint arXiv:2403.15388*, 2024. 2, 3
- [39] Enxin Song, Wenhao Chai, Guan hong Wang, Yucheng Zhang, Haoyang Zhou, Feiyang Wu, Haozhe Chi, Xun Guo, Tian Ye, Yanting Zhang, et al. Moviechat: From dense token to sparse memory for long video understanding. In *CVPR*, pages 18221–18232, 2024. 1, 2
- [40] Jianlin Su, Murtadha Ahmed, Yu Lu, Shengfeng Pan, Wen Bo, and Yunfeng Liu. Roformer: Enhanced transformer with rotary position embedding. *Neurocomputing*, 568:127063, 2024. 5
- [41] Gary J Sullivan and Richard L Baker. Efficient quadtree coding of images and video. *TIP*, 3(3):327–331, 1994. 2
- [42] Gary J Sullivan, Jens-Rainer Ohm, Woo-Jin Han, and Thomas Wiegand. Overview of the high efficiency video coding (hevc) standard. *TCSVT*, 22(12):1649–1668, 2012. 2
- [43] Keda Tao, Can Qin, Haoxuan You, Yang Sui, and Huan Wang. Dycoke: Dynamic compression of tokens for fast video large language models. In *CVPR*, 2025. 2, 3, 5, 6, 7
- [44] Robert Endre Tarjan. Efficiency of a good but not linear set union algorithm. *JACM*, 22(2):215–225, 1975. 2, 5, 7
- [45] OpenAI Team. Gpt-4o system card. *arXiv preprint arXiv:2410.21276*, 2024. 1
- [46] Zhan Tong, Yibing Song, Jue Wang, and Limin Wang. Videomae: Masked autoencoders are data-efficient learners for self-supervised video pre-training. *NeurIPS*, 35:10078–10093, 2022. 2
- [47] Hugo Touvron, Thibaut Lavril, Gautier Izacard, Xavier Martinet, Marie-Anne Lachaux, Timothée Lacroix, Baptiste Rozière, Naman Goyal, Eric Hambro, Faisal Azhar, et al. Llama: Open and efficient foundation language models. *arXiv preprint arXiv:2302.13971*, 2023. 1, 2
- [48] Du Tran, Lubomir Bourdev, Rob Fergus, Lorenzo Torresani, and Manohar Paluri. Learning spatiotemporal features with 3d convolutional networks. In *ICCV*, pages 4489–4497, 2015. 2
- [49] Zhongwei Wan, Ziang Wu, Che Liu, Jinfa Huang, Zhihong Zhu, Peng Jin, Longyue Wang, and Li Yuan. Look-m: Look-once optimization in kv cache for efficient multimodal long-context inference. *arXiv preprint arXiv:2406.18139*, 2024. 2, 3
- [50] Peng Wang, Shuai Bai, Sinan Tan, Shijie Wang, Zhihao Fan, Jinze Bai, Keqin Chen, Xuejing Liu, Jialin Wang, Wenbin Ge, et al. Qwen2-vl: Enhancing vision-language model’s perception of the world at any resolution. *arXiv preprint arXiv:2409.12191*, 2024. 1, 7
- [51] Yuxuan Wang, Cihang Xie, Yang Liu, and Zilong Zheng. Videollamb: Long-context video understanding with recurrent memory bridges. *arXiv preprint arXiv:2409.01071*, 2024. 2
- [52] Thomas Wiegand, Gary J. Sullivan, Gisle Bjontegaard, and Ajay Luthra. Overview of the h.264/avc video coding standard. *TCSVT*, 13(7):560–576, 2003. 2
- [53] Haoning Wu, Dongxu Li, Bei Chen, and Junnan Li. Longvideobench: A benchmark for long-context interleaved video-language understanding. *NeurIPS*, 37:28828–28857, 2025. 5
- [54] Junbin Xiao, Xindi Shang, Angela Yao, and Tat-Seng Chua. Next-qa: Next phase of question-answering to explaining temporal actions. In *CVPR*, pages 9777–9786, 2021. 5
- [55] Long Xing, Qidong Huang, Xiaoyi Dong, Jiajie Lu, Pan Zhang, Yuhang Zang, Yuhang Cao, Conghui He, Jiaqi Wang, Feng Wu, et al. Pyramiddrop: Accelerating your large vision-language models via pyramid visual redundancy reduction. In *CVPR*, 2025. 3, 7
- [56] An Yang, Baosong Yang, Binyuan Hui, Bo Zheng, Bowen Yu, Chang Zhou, Chengpeng Li, Chengyuan Li, Dayiheng Liu, Fei Huang, et al. Qwen2 technical report. *arXiv preprint arXiv:2407.10671*, 2024. 1
- [57] Dongjie Yang, XiaoDong Han, Yan Gao, Yao Hu, Shilin Zhang, and Hai Zhao. Pyramidinfer: Pyramid kv cache compression for high-throughput llm inference. *arXiv preprint arXiv:2405.12532*, 2024. 7
- [58] Hang Zhang, Xin Li, and Lidong Bing. Video-llama: An instruction-tuned audio-visual language model for video understanding. *EMNLP Demo Track*, 2023. 1, 2
- [59] Peiyuan Zhang, Kaichen Zhang, Bo Li, Guangtao Zeng, Jingkang Yang, Yuanhan Zhang, Ziyue Wang, Haoran Tan, Chunyuan Li, and Ziwei Liu. Long context transfer from language to vision. *arXiv preprint arXiv:2406.16852*, 2024. 1
- [60] Yuanhan Zhang, Jinming Wu, Wei Li, Bo Li, Zejun Ma, Ziwei Liu, and Chunyuan Li. Video instruction tuning with synthetic data. *arXiv preprint arXiv:2410.02713*, 2024. 1
- [61] Zijia Zhao, Haoyu Lu, Yuqi Huo, Yifan Du, Tongtian Yue, Longteng Guo, Bingning Wang, Weipeng Chen, and Jing Liu. Needle in a video haystack: A scalable synthetic evaluator for video mllms. *arXiv preprint arXiv:2406.09367*, 2024. 5

- [62] Junjie Zhou, Yan Shu, Bo Zhao, Boya Wu, Zhengyang Liang, Shitao Xiao, Minghao Qin, Xi Yang, Yongping Xiong, Bo Zhang, et al. Mlvu: Benchmarking multi-task long video understanding. In *CVPR*, pages 13691–13701, 2025. 5

## Appendix

Tabs. 11 to 14 show the absolute values for the main comparison results.

Token Budget	Method	Q. Agn.	VNBench			VideoMME			LongVideoBench			MLVU			EgoSchema			NEXT-QA			Avg.		
			Acc ↑	TTFT ↓	N <sub>v</sub> ↓	Acc ↑	TTFT ↓	N <sub>v</sub> ↓	Acc ↑	TTFT ↓	N <sub>v</sub> ↓	Acc ↑	TTFT ↓	N <sub>v</sub> ↓	Acc ↑	TTFT ↓	N <sub>v</sub> ↓	Acc ↑	TTFT ↓	N <sub>v</sub> ↓	Acc ↑	TTFT ↓	N <sub>v</sub> ↓
100%	<i>LLaVA-Video 7B</i>	✓	77.6	0.962	11149	63.1	2.039	22086	59.6	1.805	19624	70.9	2.343	25088	58.7	2.312	25069	82.9	0.659	8116	68.8	1.687	18522
50%	+ FastV		72.7	0.503	5575	61.0	1.034	11043	57.4	0.918	9812	68.3	1.164	12544	57.6	1.166	12535	82.4	0.353	4058	66.6	0.856	9261
	+ DyCoke		72.1	0.458	5386	61.5	0.912	10555	58.1	0.820	9393	69.5	1.046	11978	58.6	1.049	11969	82.1	0.330	3957	67.0	0.769	8873
	+ FrameFusion		76.2	0.471	5529	62.0	0.961	10739	59.2	0.853	9616	69.4	1.083	12138	57.7	1.088	12298	82.6	0.336	4032	67.9	0.799	9059
	+ ToMe	✓	74.1	0.518	5575	61.4	1.043	11043	58.0	0.949	9812	69.7	1.192	12544	58.7	1.199	12535	82.6	0.370	4058	67.4	0.878	9261
	+ DyCoke-stage1	✓	73.2	0.495	5386	62.0	0.981	10555	58.2	0.877	9393	69.7	1.123	11978	58.7	1.118	11969	82.4	0.350	3957	67.4	0.824	8873
	+ STTM (Ours)	✓	77.4	0.455	4804	62.6	1.021	10771	59.6	0.895	9183	69.9	1.152	12187	58.6	1.045	10737	82.5	0.322	3452	68.4	0.815	8522
30%	+ FastV		61.6	0.336	3345	59.2	0.683	6626	54.7	0.610	5887	69.3	1.620	17562	56.9	0.771	7520	81.6	0.240	2435	63.9	0.710	7229
	+ DyCoke		55.9	0.308	3548	60.7	0.598	6878	57.1	0.544	6131	67.3	0.684	7798	58.3	0.693	7792	81.5	0.229	2631	63.5	0.509	5797
	+ FrameFusion		72.4	0.292	3157	60.7	0.581	6018	57.1	0.520	5462	67.5	0.650	6768	57.4	0.657	6870	81.9	0.218	2313	66.2	0.486	5098
	+ ToMe	✓	64.1	0.364	3345	59.2	0.720	6626	56.3	0.658	5888	67.0	0.821	7527	57.4	0.834	7521	81.6	0.265	2436	64.3	0.610	5557
	+ DyCoke-stage1	✓	63.9	0.358	3548	60.0	0.700	6878	56.5	0.631	6131	68.6	0.796	7798	58.7	0.800	7792	81.7	0.256	2631	64.9	0.590	5797
	+ STTM (Ours)	✓	76.0	0.299	2649	62.3	0.640	5929	57.0	0.616	5702	68.5	0.769	7337	58.0	0.773	7285	82.0	0.235	2168	67.3	0.555	5179

Table 11. Comparison of training-free token reduction methods using LLaVA-Video-7B under 50% and 30% pre-filling token budgets.

Token Budget	Method	Q. Agn.	VNBench			VideoMME			LongVideoBench			MLVU			EgoSchema			NEXT-QA			Avg.		
			Acc ↑	TTFT ↓	N <sub>v</sub> ↓	Acc ↑	TTFT ↓	N <sub>v</sub> ↓	Acc ↑	TTFT ↓	N <sub>v</sub> ↓	Acc ↑	TTFT ↓	N <sub>v</sub> ↓	Acc ↑	TTFT ↓	N <sub>v</sub> ↓	Acc ↑	TTFT ↓	N <sub>v</sub> ↓	Acc ↑	TTFT ↓	N <sub>v</sub> ↓
100%	<i>LLaVA-OV 7B</i>	✓	68.8	0.922	11149	59.0	1.904	22086	56.3	1.712	19624	67.5	2.224	25088	61.3	2.216	25069	80.6	0.630	8116	65.6	1.601	18522
50%	+ FastV		65.6	0.467	5575	58.4	0.934	11043	56.2	0.842	9812	67.4	1.071	12544	61.0	1.080	12535	80.2	0.330	4058	64.8	0.787	9261
	+ DyCoke		64.9	0.418	5386	60.1	0.831	10555	57.9	0.740	9393	68.7	0.941	11978	61.8	0.948	11969	80.4	0.301	3957	65.6	0.697	8873
	+ FrameFusion		67.8	0.436	5568	59.8	0.865	10888	56.6	0.778	9719	68.2	0.994	12379	60.8	0.997	12511	80.8	0.312	4056	65.7	0.730	9187
	+ ToMe	✓	67.1	0.483	5575	59.8	0.963	11043	57.7	0.865	9812	68.8	1.101	12544	62.3	1.108	12535	80.1	0.343	4058	66.0	0.811	9261
	+ DyCoke-stage1	✓	65.1	0.459	5386	59.3	0.911	10555	58.2	0.821	9393	69.1	1.039	11978	61.8	1.049	11969	80.6	0.327	3957	65.7	0.767	8873
	+ STTM (Ours)	✓	71.2	0.404	4573	60.7	0.773	8579	57.7	0.804	9011	69.7	1.020	11692	61.7	0.972	10944	80.5	0.312	3628	66.9	0.714	8071
30%	+ FastV		59.2	0.303	3345	58.1	0.597	6626	55.3	0.543	5887	65.6	0.681	7526	60.9	0.694	7520	79.6	0.218	2435	63.1	0.506	5556
	+ DyCoke		53.9	0.280	3548	59.8	0.537	6878	55.9	0.488	6131	68.3	0.598	7798	62.1	0.607	7792	79.7	0.208	2631	63.3	0.453	5797
	+ FrameFusion		66.1	0.261	3263	59.0	0.499	6154	56.5	0.455	5566	66.7	0.570	6914	60.3	0.582	7251	79.9	0.195	2400	64.7	0.427	5258
	+ ToMe	✓	59.1	0.332	3345	59.8	0.649	6626	56.5	0.587	5888	69.1	0.740	7527	62.1	0.750	7521	79.5	0.240	2436	64.4	0.550	5557
	+ DyCoke-stage1	✓	58.4	0.324	3548	60.3	0.633	6878	56.2	0.577	6131	68.0	0.723	7798	62.3	0.731	7792	79.7	0.236	2631	64.1	0.537	5797
	+ STTM (Ours)	✓	70.4	0.277	2773	60.6	0.601	6264	56.6	0.570	6022	68.4	0.735	7989	61.8	0.570	5621	79.7	0.240	2577	66.2	0.499	5208

Table 12. Comparison of training-free token reduction methods using LLaVA-OneVision-7B.

Token Budget	Method	VNBench			VideoMME			LongVideoBench			Avg.		
		Acc ↑	TTFT ↓	N <sub>v</sub> ↓	Acc ↑	TTFT ↓	N <sub>v</sub> ↓	Acc ↑	TTFT ↓	N <sub>v</sub> ↓	Acc ↑	TTFT ↓	N <sub>v</sub> ↓
100%	<i>Qwen2VL 7B</i>	66.4	2.438	22025	61.8	10.745	74982	56.8	10.597	72109	61.7	7.927	56372
50%	+ ToMe	63.4	1.130	11013	61.9	4.509	37491	56.7	4.348	36054	60.7	3.329	28186
	+ DyCoke-stage1	65.1	1.049	10645	62.6	4.166	36057	57.5	4.148	34735	61.7	3.121	27146
	+ STTM (Ours)	69.8	0.726	7228	62.9	4.761	39217	57.4	4.610	37315	63.4	3.366	27920
30%	+ ToMe	56.9	0.740	6608	61.4	2.835	22496	54.7	2.600	21633	57.6	2.058	16912
	+ DyCoke-stage1	54.2	0.706	6980	61.8	2.710	23479	57.5	2.694	22649	57.8	2.037	17703
	+ STTM (Ours)	66.7	0.420	6748	62.4	2.766	23143	56.9	2.472	20022	62.0	1.886	16638

Table 13. Comparison using Qwen2VL-7B. Relative to 100% result .

Token Budget	Method	VideoMME		
		Acc ↑	TTFT ↓	N <sub>v</sub> ↓
100%	<i>LLaVA-Video 7B</i>	70.5	17.698	22086
50%	+ ToMe	70.6	8.424	11043
	+ DyCoke-stage1	70.4	8.052	10555
	+ STTM (Ours)	71.4	7.821	10082
30%	+ ToMe	68.5	5.186	6626
	+ DyCoke-stage1	69.3	5.353	6878
	+ STTM (Ours)	69.9	5.405	6897

Table 14. Comparison using LLaVA-Video-7B. Relative to 100% result .